

MEASUREMENTS OF THERMAL CONDUCTIVITY OF INDUSTRIAL NIOBIUM

F. Koechlin and P. Dolégiéviez

Département d'Astrophysique, de la Physique des Particules, de la Physique Nucléaire et de
l'Instrumentation Associée
Service Etudes des Accélérateurs

CE Saclay 91191 Gif sur Yvette

ABSTRACT

A cryostat has been built in order to measure thermal conductivities of niobium samples between 1.5 and 20 K. Thermal conductivity variations of λ versus temperature have been obtained for samples of industrial purity niobium sheets used for accelerator cavities. Electron heat conductivity measurements have been correlated with electric resistivity and RRR (residual resistivity ratio) in the range 3 K to 9 K, for RRR values varying from 40 to 250. The effect of the metal grain sizes on the phonon thermal transport between 1.6 and 2.0 K has been shown up by carrying out measurements before and after recrystallisation annealings.

Introduction

High frequency superconducting cavities are a very promising technique for high energy particle accelerators. A superconductor suitable for this purpose is niobium (critical temperature 9.2 K) used either at 4.2 K or at 1.8 - 2.0 K. Cavities may be made with bulk niobium walls, by hydroforming or deep drawing and electron beam welding niobium sheets. High frequency power is dissipated on the inner surface of the niobium wall and cooling by the liquid helium bath takes place on the outer surface. Thus, the niobium thermal conductivity in the superconducting state is an important parameter as well as the Kapitza resistance for the cavities working below 2.2 K. These quantities have already been measured [1,2,3,4]. Measurements reported here have been undertaken in order to understand heat conduction mechanisms, and qualify niobium productions by various manufacturers, or various treatments performed in the laboratory.

Experimental set-up

A vacuum vessel shown in fig.1 is immersed in liquid helium inside a classical cryostat. The sample to be measured is connected to the bottom of the vessel, a copper flange, by suitable thermal impedances. Temperatures below 4.2 K can be attained by reducing the pressure above the helium bath, down to $p \sim 1$ mbar, $T_B \sim 1.3$ K, $T_S \sim 1.5$ K (T_B is the bath temperature).

The sample temperature T_S is regulated within ± 2 mK using a P.I.D loop in which the sensor is a carbon Allen Bradley 100 Ω resistor located in the copper clamp C2. The heater H2 is a high stability resistor, located in the sample holder made of copper. Typical power in H2 is 100 mW. A silicon diode Si is also located in the sample holder in order to display its temperature.

When the sample temperature exceeds 6-7 K, carbon resistors are not found sensitive enough for small ΔT measurements and for precise regulation $s < 1$ mV/K. They are replaced by silicon diodes quite satisfactorily ($s > 20$ mV/K) in the range ($5\text{K} < T_S < 20\text{K}$).

The heat flux generating the temperature gradient along the sample is produced at the other end in the copper clamp H1. The power dissipated in resistor H1 is measured with a four wire set-up (voltage) and a precision resistor (current). The temperature gradient is deduced from measurements of the temperature variations of the copper clamps C1 and C2 when heating power by H1 is applied. C1 and C2 contain two identical Allen Bradley 100 Ω carbon resistors bonded into a copper tube or two identical silicon diodes. Thermal contact with the clamp is achieved by using a grease (Apiezon N).

Parasitic thermal exchanges, i.e. outside sample in the vacuum vessel, are minimized by :

- a vacuum isolation ($p < 10^{-6}$ mbar) making conduction losses in the gas < 100 μ W when $T_S < 13$ K
- using manganin wires and a heat dump at T_B in order to make conduction losses in the wires negligible (30 μ W for C1 and H1 at $T_S = 12$ K).

All experimental data are recorded with a data acquisition system (5 1/2 digits) and sent to a computer file system.

Measurement methods

Temperature measurements are achieved by measuring with a four wire set-up the voltage and current in each sensor C1, C2 and Si. The resistance of the sensor is deduced and the temperature is calculated at once, using a VME bus based microcomputer and a parametrization of the proper sensor resistance. For the carbon sensors, the parametrization is :

$$1/T = A + B \ln R + C(\ln R)^2$$

or [5]

$$1/T = A' + B' \ln R + C'/\ln R$$

Coefficients A, B and C are obtained by a least square fit with a set of calibration points (at least 6 points) between 1.5 K and 4.2 K, and a point near 10 K (niobium or lead superconducting transition temperature).

For the silicon diodes, the voltage at a fixed current (10 μ A) versus temperature is given by the manufacturer as a table and as a set of coefficients for an expansion in Tchebycheff polynomials. The actual diode response curve is within ± 0.5 K about the tabulated curve, and a calibration has also to be carried out [6].

Calibration measurements below 4 K have been performed using the vapor pressure of boiling helium, which is a known function of temperature. Around 10 K, resistive measurements of lead or niobium superconducting transition (7.20 and 9.25 K) were used, but, due to an uncertainty about the transition temperature (0.2 K for Nb) and to transition width $\delta T_c \sim 0.1$ K, did not yield precise calibration data. Another calibration was performed at 20 K in boiling hydrogen.

Sample preparation

The samples are rods taken out of 2 mm - thick high-purity niobium sheets. Each sample has been milled to 2x5x100 mm from a larger size piece, and chemically etched in order to remove the remaining strained metal layer (a few μm).

Experimental procedure

For each sample temperature, equilibrium without heating power H1 (but with H2 on) is reached after some time. In this state, the sample is not necessarily isothermal due to thermal losses, and temperatures T_1 , T_2 and T_{Si} (at locations C1, C2 and holder) are recorded. Then, a known power is supplied at one end of the sample by H1, in order to produce a small temperature gradient. Temperatures T'_1 , T'_2 and T'_{Si} are recorded. If w is the thermal loss flux, δT a systematic error in T_1 measurement for instance, and W the power supplied at H1, one can write [7] :

$$w = (S/L)(T_1 + \delta T - T_2)\lambda(\bar{T})$$

$$W + w = (S/L)(T'_1 + \delta T - T'_2)\lambda(\bar{T})$$

where $\lambda(\bar{T})$ is the thermal conductivity at some average temperature \bar{T} between T_1 and T_2 . Subtracting the two equations, assuming that $|T' - T| \ll |T_1 - T_2|$ so that $\lambda(\bar{T}) \sim \lambda(\bar{T})$, one obtains :

$$W = (S/L)(T'_1 - T_1 + T'_2 - T_2)\lambda(\bar{T}) = (S/L)(\Delta T'_1 - \Delta T_2)\lambda(\bar{T})$$

and $\lambda(\bar{T})$ is obtained from this equation. It can be deduced : firstly, that one has not to worry with small thermal losses ; secondly, that precise absolute temperature measurements are not necessary at locations C1 and C2 . Small calibration errors are not important but a good resolution is necessary. Consequently, high sensitivity dR/dT sensors have to be used, which is the reason to choose carbon resistors (when $1 \text{ K} < T < 7 \text{ K}$). In the actual experimental run, several values of power flux W' , W'' , W''' are applied, in order to find the best choice of T_1 , T_2 and minimize the errors. The temperature T of the sample is given by the average of the two carbon resistor measurements monitored by the silicon diode.

The last improvement in this experiment is the computer monitoring of all the experimental procedure in two temperature ranges : 1.5 to 4.2 K and 4.5 to 15 K.

RRR measurements

Samples for RRR measurements are taken out at random from each supply of niobium in order to control the purity of the final product, the 25x25 cm sheets used for deep drawing half cavities. The samples dedicated to heat conductivity measurements are taken out from the same sheets as the RRR samples. Both undergo the same preparation. This is done in order to make quantitative comparisons of RRR with heat conductivity.

The resistance of the samples is measured in another set-up, first at room temperature (293-298 K), then at 4.2 K. At 4.2 K, the samples are driven to normal state by applying a magnetic field B, slowly raised until the voltage at the sample becomes constant. This field is about 1 Tesla, depending on the sample. Corrections for magneto-resistance, and for room temperature are not applied ; it is worth noting that both effects increase the resistivity by 7 to 15%, so that, as far as one deals with the RRR, neglecting both induces an error of less than 5%, with a trend towards underestimation. As a comparison, for high RRR values (RRR > 200), the uncertainty in the measurement with a DC current of 1A is of the order of $\pm 8\%$.

Experimental results

1) as manufactured niobium

Figure 2 shows three plots of λ versus T for different qualities of niobium. This is not a comparison between the different suppliers, but rather a choice of significantly different samples.

Table 1

MATERIAL	Ingot	Sheet	Sheet	Sheet	Sheet
RRR	265	255	198	194	40
$\lambda(4K)$ W/ mK	54	50	46	44	11
RRR/ $\lambda(4K)$	4.86	5.1	4.26	4.35	3.64
$\lambda(2K)$ W/ mK	10	7	6.6	6.4	6.0
$\lambda(2K)/\lambda(4K)$	0.175	0.14	0.14	0.15	0.54

The steep increase of λ versus T, when T/T_C is lower than one ($T_C=9.25$ K) can be noticed, and when T is lower than 3 K a slight bump can be observed. Table 1 displays the main numerical results that can be deduced from the figure. It can be seen that :

- $\lambda(4$ K) increases almost linearly with the RRR
- The ratio $RRR/\lambda(4.2)$ is close to 4, but increases with the RRR
- $\lambda(2$ K) is almost independent of the RRR for the sheets and is 50% higher for the ingot.
- The ratio $\lambda(2$ K)/ $\lambda(4.2)$ is of the order of 1/6 to 1/7, which is an important drawback for evacuating heat at such a temperature. Happily the surface resistances have a larger ratio (~ 30), so that the net balance for RF cavities favors operation at 1.8-2 K.

These results are consistent with the usual description of heat conduction by the superconductor metals and the BCS theory.

Electron heat conduction

When T is larger than 3 K, the heat is carried by the electrons scattered by impurities and by the lattice (electron phonon interaction), as in a normal metal. However, those electrons which have condensed into Cooper pairs do not contribute any longer to momentum transport, that is to heat conductivity ; the non-paired or normal electrons do contribute. Their number decreases exponentially with T, roughly as $\exp(-\Delta/kT)$. So that the electron contribution λ_{es} to the heat conductivity in the superconducting state can be written

$$\lambda_{es} = [\rho_0/L_0 T + aT^2]^{-1} g(\Delta, T_C, T)$$

where ρ_0 is the residual resistivity due to electron scattering by the impurities, L_0 is the Lorentz constant in Wiedemann-Frantz law, a the coefficient of electron phonon momentum exchange, g is the ratio of superconducting to normal state heat conductivity ; $g = 1$ when $T > T_C$, $g \sim \exp(-1.9 T_C/T)$ when $T < T_C$. This explains the steep decrease of λ (fig.2) when $T < 9$ K. On the other hand the phonon resistance term is one half the impurity term when λ_{en} is a maximum, $T_m \sim 9$ to 15 K, so that at 4 K the phonon term is $\sim 3 \cdot 10^{-2}$ times the impurity term and can be neglected. Thus, if we consider $\lambda_{es}(4K)$, we can simplify and write :

$$\lambda_{es} \approx (L_0 T / \rho_0) \cdot g(\Delta, T_C, 4.2)$$

and since :

$$\rho_0 = \rho(300)/RRR$$

$$g(\Delta, T_C, 4.2) = 0.25$$

one has

$$\lambda_{es} \approx L_0 / \rho(300) \cdot 4.2 \times 0.25 \cdot RRR \sim RRR/5$$

The value of $RRR/4$ had been given by Padamsee [8] and was verified experimentally for RRR values lower than 100. Indeed, Kadanov and Martin [11] have shown that the function $g(T)$ has a slight dependence on the ratio of the phonon term to the impurity term, that is g is smaller when the RRR is higher, so that the ratio RRR/λ should increase with the RRR as is observed here. In the present case however, Kadanov parameter is smaller than one, and the variation of g with the RRR at $T = 4.2$ K is negligible in their calculation.

At lower temperatures, $T \sim 2$ K for instance, $g(T)$ is very small ($g(2 K) \sim 0.007$), that is the electron contribution to heat transport is insignificant, and the heat transport by phonons is the dominant term, which is a peculiarity of superconductors among metals.

Phonon heat conduction

When the normal electron population becomes very low ($T < 3$ K, $g < 0.07$) the phonon heat conduction can be observed. These phonons are scattered by normal electrons, their contribution is enhanced when these are a few, and then is damped when the temperature increases. Another cause of damping exists when the phonon mean free path L is comparable to the dimensions of the specimen. Thus the phonon contribution has a maximum, which is the slight bump or the plateau seen in figure 2 on the three curves.

According to preceding results [2,4], a stronger bump due to phonons heat conductivity could be expected. It can be noticed however that the grain size of the sheets is in the range 50-70 μm in order to achieve successfully the deep drawing of cavities.

The lattice heat conductivity in the superconducting state λ_{gs} can be estimated by adding two thermal resistances :

$$1/\lambda_{gs} = 1/CLT^3 + 1/\lambda_{gs}^*$$

where C is a constant, L the phonon mean free path, λ_{gs}^* the BCS term which takes into account the momentum exchange of phonons with free electrons. The phonon mean free path is independant of temperature in the considered range, and is determined by the lattice defects or the specimen boundaries [12].

On the other hand, the BCS theory [9] gives the variation as a function of temperature of $\lambda_{gs}^*/\lambda_{gn}$, where λ_{gn}^{-1} is the thermal resistance in the normal state.

$$\lambda_{gs}^* = \lambda_{gn} f(\Delta, T_C, T)$$

where Δ is the superconductor energy gap. The function f is roughly given by :

$$f(\Delta), T_C, T \sim \exp [\Delta(T)/kT] \sim \exp [\Delta(O)/kT]$$

in our temperature range [1]. The quantity $\Delta(O)/kT = y$ can be written $y = 1.98 T_C/T$. Now, λ_{gs} can be written :

$$\lambda_{gs} = CLT^3 \{ 1 + CLT^3/[\lambda_{gn} \exp(y)] \}^{-1}$$

If we take $T = 1.85$ K, $T/T_C = 0.2$, then $\exp(y) = 2.10^4$ so that, for T smaller than ~ 2.5 K, the lattice heat conductivity is proportional to the phonon mean free path L . One can think that the phonon mean free path L is related to the grain average diameter, and that the weakness of the bumps in fig. 2 is a consequence of the small grain size. On the contrary, instead of having been cold worked, the specimens exhibiting the high phonon peak have been annealed, a procedure which increases the grain dimensions, making L and thus λ_{gs} increase enough to make a bump. These features have been noticed by Wasserbach [1] who applied plastic deformations to high purity specimens in order to reduce the grain dimensions.

2) Annealed niobium

In order to check the grain size effects on the phonon heat conductivity, two annealing experiments have been performed, one at a temperature of 1200°C, the other at 750°C. The residual pressure in the furnace was $2 \cdot 10^{-6}$ mbar (oil diffusion pump with liquid nitrogen trap). The residual resistance ratio and the thermal conductivity profile were measured before and after annealing. Results are shown in figures 3 and 4, and summarized in table 2 :

Table 2

Sample	Anneal.	Param.	RRR before	RRR after	$\lambda(2K)$ before	$\lambda(2K)$ after
D 01	1200°	2 h 20	255	80	7 W/mK	40 W/mK
B 20	"	"	125	63	-	-
HT	750°	1 h 30	194	186	6.5	13
WT	"	"	40	40	6	10
HT	1000°	2 h 00	186	103	-	-

The annealing at 750°C (fig.3) has improved the heat conductivity of sample HT by a large amount in the phonon conduction region (a factor 2 at 2K) and by a small amount in the lower temperature part of the electron region (+ 20% at 4K). On the other hand, the small degradation of the RRR (4%) is in the error range. Note that the sample WT of RRR = 40 has a heat conductivity comparable to that of sample HT at 2K.

The hydrogen concentration in the bulk niobium should have decreased, because the equilibrium concentration with 10% of the furnace residual pressure is 2 at ppm, also because the diffusion time for a thickness of 2mm is very short. On the contrary the nitrogen equilibrium concentration in the same conditions is 2900 at ppm, and almost no outgassing occurs at 750°. Oxygen is in the same case. So, one can conclude that either hydrogen outgassing, or an increase of the phonon mean free path due to grain dimensions, or both, is responsible of the increase of heat conductivity between 1K and 4K.

The annealing at 1000°C of the same sample reveals a significant degradation of the RRR. This is due to absorption of oxygen from the residual gas, at a rate of $1 \cdot 10^{-4}$ at % per minute that is 135 at ppm after two hours (partial pressure : 50%). For a final RRR of 103 the absorbed concentration of oxygen has to be 140 at ppm. These figures are consistent enough to confirm the hypothesis.

The 1200°C annealing in the same furnace (fig. 4) shows an enormous increase (x7) of the heat conductivity of the niobium sheet at 1.8 - 2.0 K as well as a strong degradation of heat conductivity and RRR at 4 K (λ ; 2 ; RRR ; 3). As before, the absorption of oxygen up to an amount of 275 ppm, which takes 240 min. with 50% partial pressure, can explain the ultimate RRR of 80.

Micrographies of the sample performed before and after the annealing [13] show that the metal grain diameter has increased from 50-70 μm to 400-500 μm . According to Casimir theory of phonon heat conduction [12], the conductivity is proportional to the phonon mean free path ; in the present case $\lambda(2\text{K})$ has been multiplied by 7 and the grain average diameter by 7-8. This is a strong convergence which leads to think that the phonon mean free path and thus the heat conductivity of superconducting niobium are directly dependent on the metal grain dimensions, when $T < 2.5 \text{ K}$, that is $T/T_C < 0.3$.

Conclusion

High purity industrial niobium is required in order to have a good thermal conductivity by electrons when $T > 2.5 - 3 \text{ K}$. However, it is shown that, in the range $T \sim 1.8 - 2.0 \text{ K}$, the low value of heat conductivity by phonons is due to small grain dimensions. Moderate temperature annealing ($800^\circ\text{C} < T < 1200^\circ\text{C}$) can increase considerably the grain sizes and the heat conductivity at 2 K, provided that the furnace works with a partial pressure of oxygen less than 1.10^{-7} mbar. Nitrogen also has to be avoided, but is less deleterious than oxygen when $T < 1500^\circ\text{C}$.

Such a heat treatment would allow higher HF fields in those cavities where a diffuse quench is the phenomenon limiting the accelerator field at 2 K.

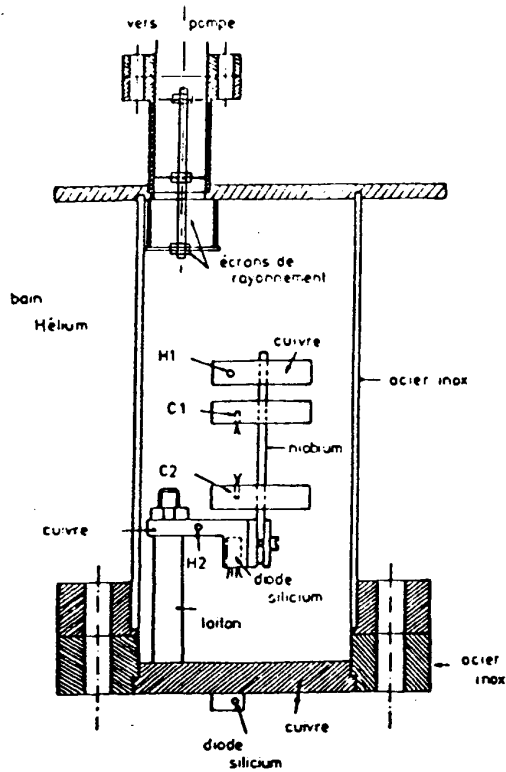
Acknowledgements

The authors wish to thank Y. BOUDIGOU for his efficient help, J. FOUAN and J. PAPE of CEA for lending and operating the oven, MM. JUNQUERA and LIEBE of CNRS for their help in sensor calibration, L. WARTSKI of CNRS and all the GECS group for encouraging this work.

References

- [1] WASSERBACH W., Phys. Sta. Sol., 84, 205 (1977).
- [2] KATHLEEN REMPEL KRAFFT Thesis Cornell University, USA (1983).
- [3] SCHOPPER A., WEINGARTEN W., Report CERN/EF/RF 83-7 (1983).
- [4] MAUSER H.G., report D 85-19 (1985), Bergische Univ. Gesamthochsch. Wuppertal, FRG.
- [5] CLÉMENT J.R. and QUINNEL E.H., Rev. Sci. Inst. 23, 213 (1952).
- [6] LAKE SHORE Cryotronics Inc., Westerville Ohio, U.S.A.
- [7] LOCATELLI M., B.I.S.T, 215, 39 (1976) [CEA Paris France].
- [8] PADAMSEE H., 2nd Workshop on RF Superconductivity, 339 (1984) [H. LENGELER, CERN, editor].
- [9] BARDEEN J., RICKAYZEN G., TEWORDT L., Phys. Rev. 113, 982 (1959).
- [10] CONNOLY A., MENDELSSOHN K., Proc. Roy. Soc. A 266, 429 (1962).
- [11] KADANOV L.P., MARTIN P. ; Phys. ReV. 124,670 (1961).
- [12] CASIMIR B., Physica 5,495 (1938).

- [13] DOLEGIEVIEZ P., KOEHLIN F., Proceedings of ICMAS-90 (Grenoble, oct. 90)
[A. NIKU-LARI, II.T.T., Paris France, editor].



SCHEMA DE L'ENCEINTE DE MESURE

Figure 1

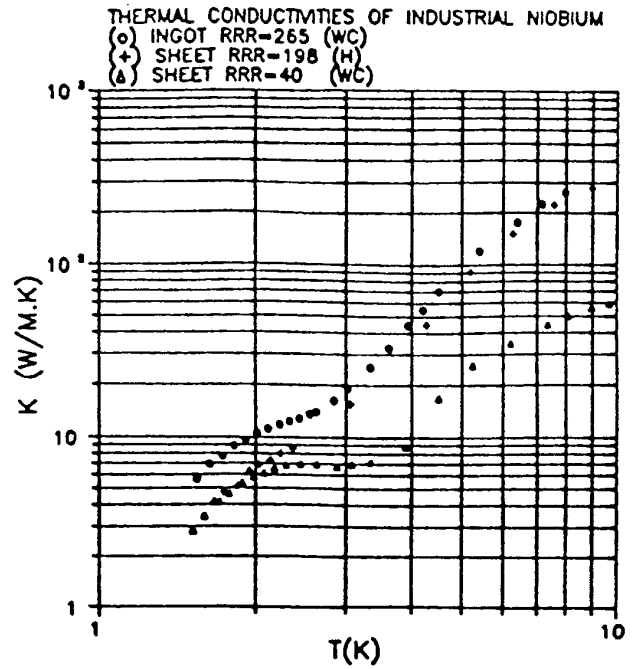


Figure 2

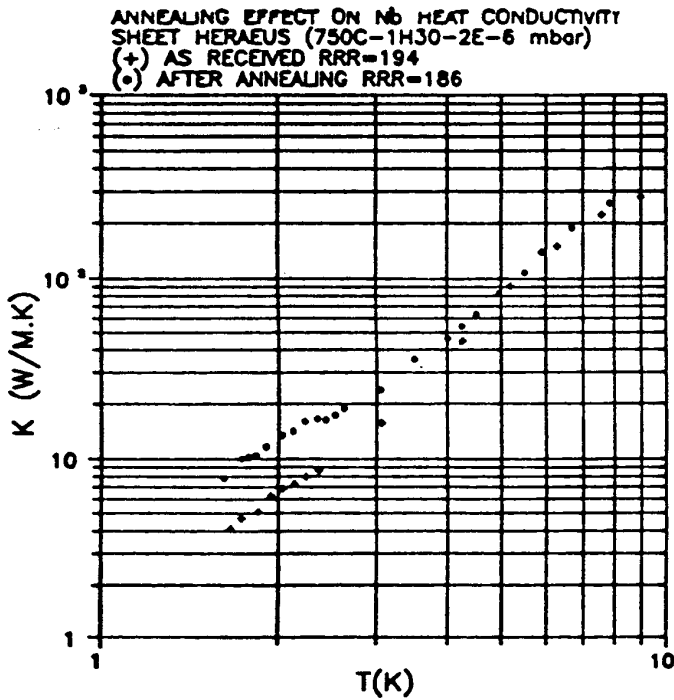


Figure 3

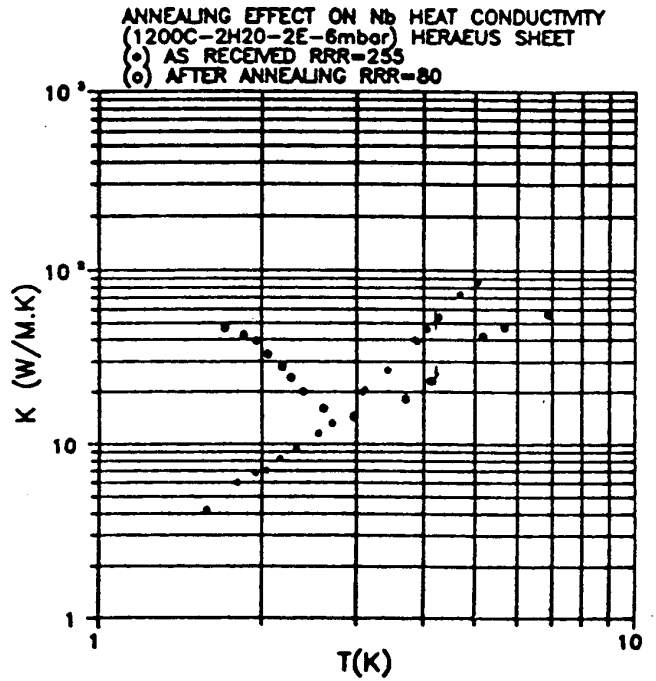


Figure 4